J. Environ. Nanotechnol.
Volume 3, No.2 pp. 108-121
ISSN (Print) : 2279-0748
ISSN (Online) : 2319-5541
doi : 10.13074/jent.2014.03.142072

Experimental Spectroscopic (FT-IR, FT-Raman, NMR) and DFT Studies of 7-methoxy-4-bromomethylcoumarin

N. Prabavathi [1]*, N. Senthil Nayaki[2]

[1*,2]*Department of Physics, Sri Sarada College for women (Autonomous), Salem, TN, India.*

Received : 10.04.2014 Accepted : 23.05.2014

Abstract

The vibrational fundamental modes of 7-methoxy- 4-bromomethylcoumarin (7BMC) have been analyzed by combining FTIR, FT-Raman and quantum chemical calculations. The structural parameters of the compound are determined from the optimized geometry by B3LYP method with 6-311++G (d, p) basis set. The harmonic vibrational frequencies were calculated and the scaled values have been compared with experimental FTIR and FT-Raman spectra. ^{1}H and ^{13}C NMR spectra have been analyzed and ^{1}H and ^{13}C nuclear magnetic resonance chemical shifts are calculated using the gauge independent atomic orbital (GIAO) method. The theoretical UV–VIS spectrum of the compound and the electronic properties, such as HOMO (highest occupied molecular orbital) and LUMO (lowest occupied molecular orbital) energies were performed by time-dependent density functional theory (TD-DFT) approach. Information about the size, shape, charge density distribution and site of chemical reactivity of the molecule have been obtained by mapping electron density isosurface with molecular electrostatic potential (MESP). The change in electron density (ED) in the σ^* antibonding orbitals and stabilization energies E(2) have been calculated by natural bond (NBO) analysis to give clear evidence of stabilization originating in the hyper conjugation of hydrogen–bonded interactions.

Keywords: *DFT; HOMO-LUMO; NMR; Vibrational spectra; 7-methoxy-4-bromomethylcoumarin .*

1. INTRODUCTION

Coumarins are an important class of oxygen heterocycles, widespread in the plant kingdom (Borges *et al.* 2005). Coumarins are of great interest due to their biological properties. In particular, their physiological, bacteriostatic and anti-tumour activities make these compounds more attractive in the field of medicine. They have been shown to be useful as antitumoural and anti-HIV agents. Some coumarins emit a strong fluorescence, on the substitution of various functional groups at different positions, with a pronounced charge transfer (CT) character (Prasad *et al.* 2013). 4-methyl coumarins have been found to possess choleretic, analgesic, anti-spermatogenic, anti-tubercular and diuretic properties. 7-methoxycoumarin naturally occurs in chamomile and presents a alsamic sweet odor. 4-methyl-7-methoxycoumarin is used as a fluorescent label for high performance liquid chromatography (Prabavathi and Senthil Nayaki, 2014). 4-bromomethyl-7-methoxycoumarin is used as a fluorescent label for fatty acids. It has been used in the flurometric analysis of prostaglands and a wide range of naturally occurring acids, including bile and thromboxane B2 (Alekseev, 1981). Owing to the importance listed above, a comprehensive DFT study has been performed on the titled molecule.

N.Prabavathi Tel. No.: +909791847378
E–mail: n.prabavathi@yahoo.co.in

2. EXPERIMENTAL DETAILS

The compound under investigation 7-methoxy-4-bromomethyl coumarin (7BMC) was purchased from the Sigma Aldrich Company and used as such without any further purification. The room temperature FT-IR spectrum of 7BMC was measured in the region 4000–400 cm^{-1} on BRUKER IFS 66V spectrometer usingKBr pellet with the spectral resolution ±1 cm^{-1}. The FT-Raman spectrum of the chosen molecule was recorded in the region 4000–100 cm^{-1} with BRUKER RFS 100/s Raman module, equipped with an Nd:YAG laser source, operating at 1064 nm linewidth 150 mW power. The reported wavenumbers are expected to be accurate to within ±1 cm^{-1}.

^{1}H and ^{13}C nuclear magnetic resonance (NMR) (400 MHz; $CDCl_3$) spectra were recorded on a Bruker HC400 instrument. Chemical shifts are reported in parts per million scale (delta scale) downfield from tetramethylsilane.

3. COMPUTATIONAL DETAILS

The quantum chemical calculation of 7BMC has been performed using Gaussian 09 program (Benito Reyes-Trejo *et al*. 2014) at the B3LYP level, supplemented with the standard 6-311++G** basis set. The optimized geometries corresponding to the minimum potential energy surface have been obtained by solving self-consistent field equation iteratively. Harmonic vibrational wave numbers have been calculated using analytic second derivatives to confirm the convergence to minima on the potential energy surface and to evaluate the zero-point vibrational energy. Multiple scaling of the force field has been performed by the scaled quantum mechanical (SQM) procedure, to offset the systematic errors caused by basis set incompleteness, neglect of electron correlation and vibrational anharmonicity. Normal coordinate analysis on 7BMC has been performed to obtain full description of the molecular motion pertaining to the normal modes using the MOLVIB-7.0 program. The calculated analytic force constants are used by MOLVIB in the calculation of vibrational frequencies by diagonalization of dynamical matrix. These force fields obtained in cartesian coordinates and dipole derivatives with respect to atomic displacements were extracted from the archive section of the Gaussian 09 output and are transformed to a suitably defined set of internal coordinates (the 'natural coordinates'). The Raman activities (S_i) calculated by Gaussian 09 program have been suitably adjusted by the scaling procedure of MOLVIB and subsequently converted to relative Raman intensities (I_i) using the following relationship derived from the basic theory of Raman scattering.

$$I_i = \frac{f(\nu_0 - \nu_i)^4 S_i}{\nu_i [1 - \exp(-hc\nu_i / kT)}$$

where v_0 is the exciting frequencuy(in cm^{-1} units), v_i is the vibrational wave number of ther ith normal mode, *h*, *c*, *k* are the fundamental constants and *f* is a suitably chosen common normalization factor for all peak intensities.

The symmetry of the molecule is also helpful in making vibrational assignments. By combining the results of the Gauss view program with symmetry considerations, vibrational frequency assignments are made with a high degree of confidence. There is always some ambiguity in defining internal coordinates. However, the defined coordinates form a complete set and matches quite well with the motions observed using the Gauss view program.

The natural bonding orbital (NBO) calculations were performed using NBO 3.1 program, implemented in the Gaussian 09 package at the DFT/B3LYP level. NBO helps to understand various second order interactions between the filled orbitals of one subsystem and the vacant orbitals of another subsystem, which is a measure of the intermolecular delocalization and hyper conjugation. The hyper conjugative interaction energy was deduced from the second-order perturbation approach (Prabavathi *et al*. 2013).

$$E^{(2)} = \Delta E_{ij} = q_i \frac{F^2_{(i,j)}}{\varepsilon_{j-}\varepsilon_i}$$

where $F_{i,j}$ is the Fock matrix element between i and j NBO orbitals ε_i and ε_j are the energies of σ and σ* NBO's, and q_i is the population of the donor σ orbital.

4. RESULTS & DISCUSSION

4.1 Molecular Geometry

In order to figure out the minimum energy conformer of the titled molecule, potential energy surface (PES) scan has been performed on the dihedral angle Br16-C13-C4-C3. Structure optimization is done for the minimum energy conformer. The optimized structure of 7BMC with numbering scheme for the atoms is presented in Fig.1 and it belongs to C_1 point group symmetry with energy of about -3224.583 Hartrees. The optimized structural parameters like bond length, bond angle and the dihedral angle of 7BMC determined by B3LYP method with 6–311++G** basis sets are summarized in the Table 1. All the C-H bond length of 7BMC averages to 1.08 Å except methoxy and bromomethyl groups, where it averages to 1.09 Å. In 7BMC the O11-C2bond length is 1.2 Å and it coincides with the reported C-O bond length 1.2 Å of 7-methoxy-4-methyl coumarin, 3-acetylcoumarin and 3-cyano methyl coumarin (Prabavathi and Senthil Nayaki, 2014). The ring C-O bond length is usually 1.43 Å (Arjunan *et al.* 2013). But, a reduction in bond length (C2-O1= 1.39 and C9-O1=1.36 Å) observed in the present investigation is due to the fusion of benzene ring with the α–pyrone ring through O1 atom (Prabavathi and Senthil Nayaki, 2014). The substituent plays a vital role on the structural and electronic properties of the molecules. The bromomethyl and methoxy group substitution affect the regular hexagonal structure of their respective rings, which is evident from the observed bond angles. The decrease in bond angle C7-C8-C9 (118°) in turn reduces the C7-O19 bond length (1.35 Å).

4.2 Hyperpolarizability

The first hyperpolarizability (β_0) and its components of the 7BMC, calculated based on the finite-field approach are given in Table 2. The ground-state dipole moment and the hyperpolarizability are governed by the extent of π electron delocalization, which in turn depends on the structural details of the molecules. In the current work the dipole moments, as well as first hyperpolarizabilities are nonzero as the equilibrium geometries are noncentrosymmetric. The dominant direction of charge delocalization is found to be along β_{xxx}. As the β_{tot} value of 7BMC is greater than urea (Sebastain *et al.* 2011), this can serve as a good nonlinear optical material [NLO].

4.3 Analysis of Molecular Electrostatic Surface Potential (MESP)

Molecular electrostatic potential (MESP) mapping is very useful in the investigation of the molecular structure with its physiochemical property relationships (Arjunan *et al.* 2014). The MESP has been also employed as an information tool of chemistry to describe different physical and chemical features, including non-covalent interactions in complex biological system. It provides a visual method to understand the relative polarity of the molecule. The different values of the electrostatic potential are represented by different colors; red represents the negative regions of electrostatic potential, blue represents the positive regions of electrostatic potential

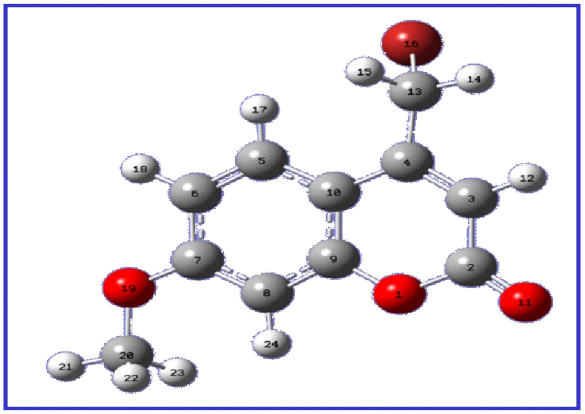

Fig. 1: Molecular structure of 7-methoxy-4-bromomethylcoumarin with atom numbering scheme.

Table 1. Optimized geometrical parameters of 7-methoxy-4-bromomethylcoumarin.

Bond length	Value (Å)	Bond angle	Value (°)	Torsional angle	Value (°)
C2-O1	1.39	C3-C2-O1	115.72	C4-C3-C2-O1	0
C3-C2	1.45	C4-C3-C2	122.97	C10-C4-C3-C2	0
C4-C3	1.36	C10-C4-C3	119.28	C5-C10-C4-C3	180
C10-C4	1.45	C5-C10-C4	125.52	C6-C5-C10-C4	180
C5–C10	1.41	C6-C5-C10	121.55	C7-C6-C5-C10	0
C6-C5	1.38	C7-C6-C5	120.01	C8-C7-C6-C5	0
C7-C6	1.41	C8-C7-C6	120.01	C9-C8-C7-C6	0
C8-C7	1.39	C9-C8-C7	118.93	O11-C2-O1-C9	180
C9-C8	1.39	O11-C2-O1	117.92	H12-C3-C2-O1	180
O11-C2	1.20	H12-C3-C2	115.02	C13-C4-C3-C2	180
H12-C3	1.08	C13-C4-C3	118.01	H14-C13-C4-C3	0
C13-C4	1.50	H14-C13-C4	110.57	H15-C13-C4-C3	-120
H14-C13	1.09	H15-C13-C4	111.70	Br16-C13-C4-C3	120
H15-C13	1.09	Br16-C13-C4	114.97	H17-C5-C10-C4	0
Br16-C13	1.98	H17-C5-C10	119.6	H18-C6-C5-C10	180
H17-C5	1.08	H18-C6-C5	121.31	O19-C7-C6-C5	180
H18-C6	1.08	O19-C7-C6	115.7	C20-O19-C7-C6	180
O19-C7	1.35	C20-O19-C7	118.89	H21-C20-O19-C7	180
C20-O19	1.43	H21-C20-O19	105.69	H22-C20-O19-C7	61
H21-C20	1.09	H22-C20-O19	111.06	H23-C20-O19-C7	-61
H22-C20	1.09	H23-C20-O19	111.27	H24-C9-C8-C6	180
H23-C20	1.09	H24-C8-C7	122.98		
H24-C8	1.08				

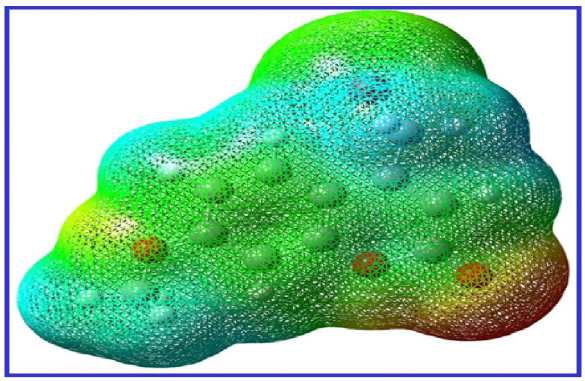

Fig. 2: The total electron density isosurface mapped with molecular electrostatic potential of 7-methoxy-4-bromomethyl coumarin

and green is the region of zero potential. Potential increases in the order red < orange < yellow < green < blue (Sheela *et al.* 2014). The projection of such a mapped electrostatic potential surface for the title molecule is given in Fig. 2. In the present work, the calculated result shows that the negative potentials are mainly over the electro negative oxygen atoms O1 and O11. The dominance of blue colour over the hydrogen atoms of 7BMC indicates the presence of positive potential near hydrogen atoms. Thus the hydrogen atoms are the preferred sites for nucleophilic reactivity. The extensive delocalization of charges from the ring carbon atoms and bromine atom is proved by the prevalence of green colour over these atoms.

4.4 Thermodynamic Properties

The zero point energies, thermal correction to internal energy, enthalpy, Gibbs free energy and entropy and heat capacity for a molecular system were computed from the Gaussian frequency calculations. The computed thermodynamic parameters are listed in Table 3. On the basis of vibrational analysis, the thermodynamic functions such as heat capacity, entropy (S) and enthalpy change ($\Delta H_{0\rightarrow T}$) at constant pressure (Cp), for 7BMC were also determined and are listed in Table 4. The graph showing the correlation of heat capacity, entropy (S) and enthalpy change ($\Delta H_{0\rightarrow T}$) with temperature at constant pressure (Cp), is delineated in Fig. 3. All the computed thermodynamic functions of

Table 2. Calculated all β components and $\beta_{\tau o t}$ (x10-30) value of 7-methoxy-bromomethylcoumarin

β -components	B3LYP/6-311++G** 7-methoxy-4-bromomethylcoumarin
β_{xxx}	-804.52
β_{xxy}	521.46
β_{xyy}	-334.93
β_{yyy}	-124.50
β_{xxz}	10.25
β_{xyz}	-46.85
β_{yyz}	43.20
β_{xzz}	-6.80
β_{yzz}	-32.49
β_{zzz}	6.71
B_{total}(esu)	$10.4*10^{-30}$

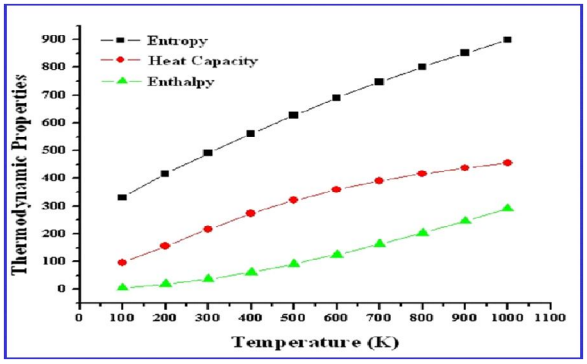

Fig. 3: Temperature dependence of heat capacity, Entropy and Enthalpy change at constant pressure of 7-methoxy-4-bromomethylcoumarin

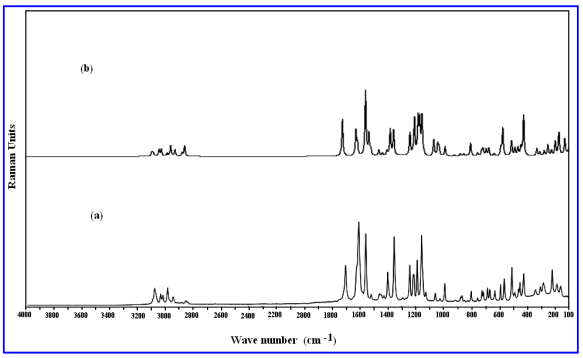

Fig. 4: Comparison of observed and calculated FT-RAMAN spectra of 7-methoxy-4-bromomethyl coumarin (a) observed and (b) calculated with B3LYP/ 6–311++G**

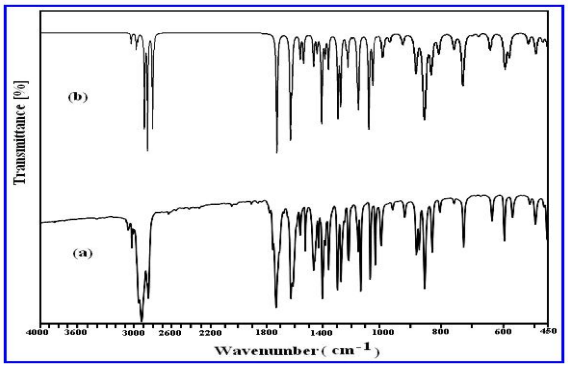

Fig. 5: Comparison of observed and calculated FTIR spectra of 7-methoxy-4-bromomethylcoumarin (a) observed and (b) calculated with B3LYP/6–311++G**

7BMC increases steadily with temperature, ranging from 100 to 1000 K, due to the enhancement of the molecular vibration with increase in temperature.

Here, all the mentioned thermodynamic calculations were done in gas phase. As per the second law of thermodynamics in thermo chemical field (Sebastian *et al*. 2013), these calculations can be used to compute the other thermodynamic energies and helps to estimate the directions of chemical reactions.

4.5 Spectral Analysis

Detailed description of vibrational modes can be given by means of normal coordinate analysis (NCA). For this purpose, the standard internal coordinates (containing redundancies) were constructed. From these, nonredundant set of local symmetry coordinates were constructed by suitable linear combinations of internal coordinates Elbert *et al*. (1985). In agreement with the C1 symmetry, the 66 normal modes of 7BMC are distributed among the symmetry species as

$$T_{3N-6} = 45\,(\text{in-plane}) + 21\,(\text{out-of-plane})$$

The detailed vibrational assignment of fundamental modes of the titled molecule was made unambiguously with the help of Gauss view program and the PED (potential energy distribution) obtained

Table 3. The calculated thermodynamic parameters of 7-methoxy-4-bromomethylcoumarin.

Structural parameters	6-311++G**
SCF energy (Hartrees)	-3224.5831
Total energy (thermal), E_{total} (kcal mol^{-1})	119.658
Heat capacity at const. volume, Cv (cal $mol^{-1}K^{-1}$)	49.573
Entropy, S (cal $mol^{-1}K^{-1}$)	117.043
Vibrational energy , E_{vib} (kcalmol^{-1})	117.881
Zero-point vibrational energy, E_0 (kcal mol^{-1})	111.382
Rotational constants (GHz)	
A	0.58843
B	0.28876
C	0.20058
Dipole moment (Debye)	
μ_x	1.4203
μ_y	-3.3411
μ_z	1.5896
μ_{total}	3.9632

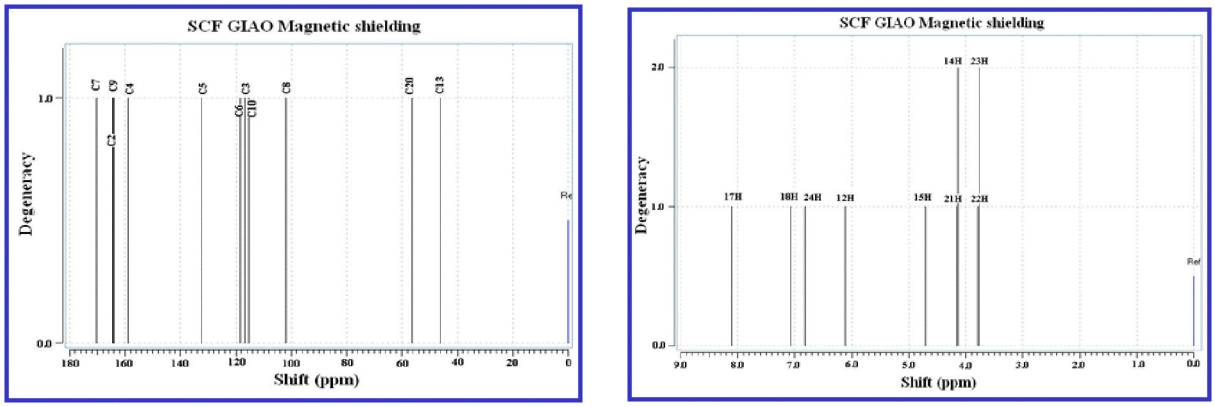

Fig. 6: Theoretically simulated NMR spectrum of ^{13}C and ^{1}H of 7-methoxy-4-bromomethyl coumarin

during the scaling procedure with Molvib Program. These assignments along with calculated IR, Raman intensities and normal mode description (characterized by PED) are reported in Table 5. The observed and simulated FT-Raman and FT-IR spectra of 7BMC were produced in common frequency scales and are presented in Figs. 4 and 5 respectively. The RMS error between unscaled and experimental frequencies was reduced to 4.7 by applying refinement of scaling factors and optimizing via least square refinement algorithm.

4.5.1 C-C vibrations

In the present work, the experimental and theoretical skeletal (ring CC) vibrations were assigned in the region 915-1630 cm^{-1} (Prabavathi and Senthilnayaki, 2014). The peaks observed at 1621, 1607, 1557, 1400, 1357, 1293, 1214, 1057 and 917 cm^{1} in FT-IR spectrum are assigned to CC-stretching vibrations. Except three all these bands were present in FT-Raman spectrum. The experimental data shows excellent agreement with the theoretical data. The CC in-plane

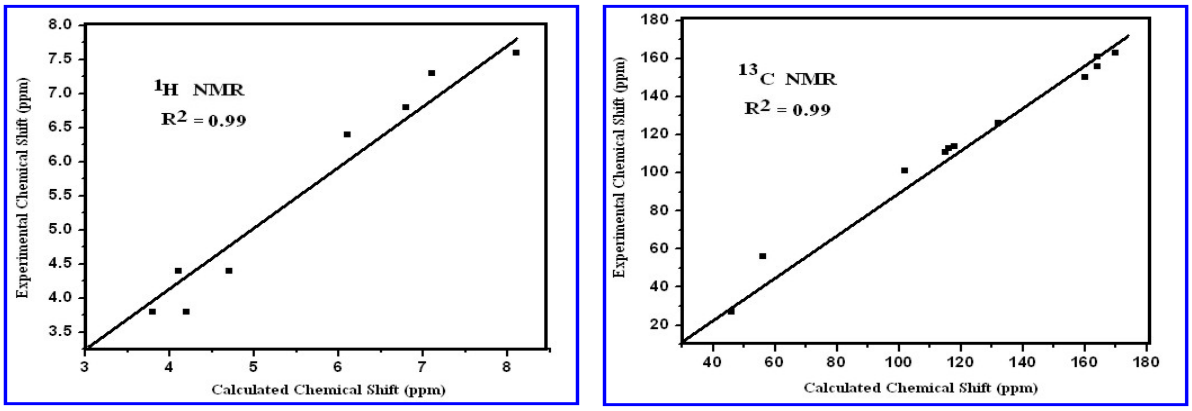

Fig. 7: The linear regression between the experimental and theoretical ^{1}H and ^{13}C NMR chemical shifts of 7-methoxy-4-bromomethylcoumarin.

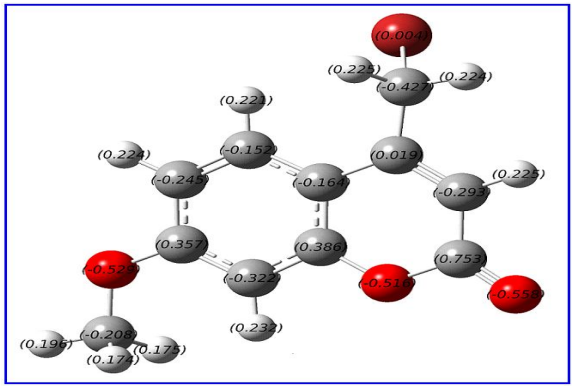

Fig. 8: Illustration of Natural atomic charges of 7-methoxy-4-bromomethylcoumarin

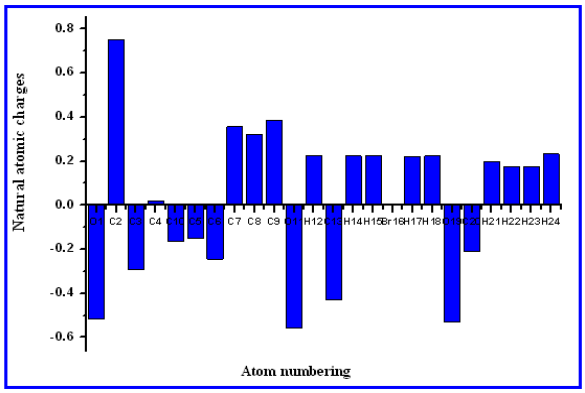

Fig. 9: Natural atomic charges analysis chart

Table 4. The temperature dependence of thermodynamic parameters of 7-methoxy-4-bromomethylcoumarin

Temp. (K)	Entropy (J mol^{-1} K^{-1})	Heat capacity (C_p, J mol^{-1} K^{-1})	Enthalpy (KJ mol^{-1})
100	331.45	96.14	6.27
200	416.40	155.90	18.86
300	491.16	216.84	37.51
400	561.47	273.47	62.08
500	627.81	321.27	91.90
600	689.93	359.97	126.03
700	747.85	391.17	163.65
800	801.80	416.60	204.08
900	852.12	437.60	246.82
1000	899.16	455.16	291.48

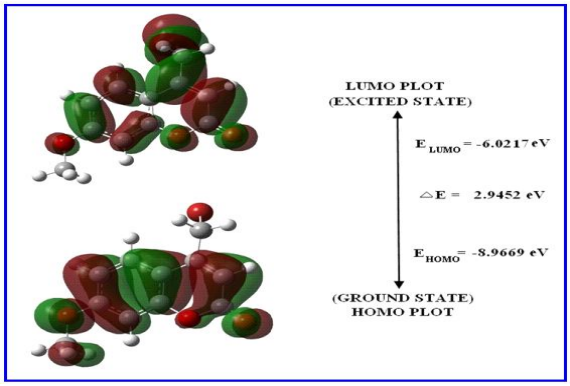

Fig. 10: The atomic orbital compositions of the frontier molecular orbital for 7-methoxy-4-bromomethylcoumarin

Table 5. Observed and B3LYP / 6-311++G level calculated vibrational frequencies (in cm $^{-1)}$ of 7-methoxy-4-bromomethylcoumarin**

S.No.	Observed frequencies (cm^{-1})		Calculated frequencies (cm^{-1}) with B3LYP/ 6-311++G** level				PED (%) among type of internal coordinates
	Infrared	Raman	Unscaled	Scaled	IR$^{a}(A_i)$	Raman$^{b}(I_i)$	
1	3085	-	3225.4	3085.0	61.31	76.400	CH(99)
2	-	3075	3212.5	3075.0	1.521	64.391	CH(97)
3	3030	3033	3205.3	3033.0	90.06	111.830	CH(99)
4	3010	3017	3197.5	3017.0	41.68	117.562	CH(97)
5	-	2975	3155.8	2975.0	2.165	50.766	CH2ASS(80),CH2SS(19)
6	2950	2942	3144.2	2950.0	523.01	172.524	CH2SS (62),CH2ASS(19),
7	2920	-	3091.8	2920.0	646.00	97.144	OCH3op(79), OCH3ip (20)
8	2860	2867	3079.1	2867.0	528.54	51.425	OCH3ip(78),OCH3op(21)
9	-	2850	3015.2	2850.0	40.626	149.173	OCH3SS(80),OCH3op(17)
10	1720	1702	1799.4	1719.9	703.098	173.554	CO(80),bring1(9),CC(7)
11	1621	-	1654.7	1622.8	584.229	105.275	CC(32),CO3(18),bCCH(15),CC (14)
12	1607	1608	1641.4	1611.3	261.143	48.412	CC(29),CC(22),CC(18),bring2(6)
13	1557	1550	1580.3	1554.9	141.656	254.462	CC(34),CC(27),bCCH(10),CC25)
14	1521	-	1539.7	1527.6	166.592	81.078	CC(32),bCCH(22),CC(11),CO(10)
15	-	1517	1504.0	1516.8	3.127	20.754	OCH3ipb(88),OCH3ips(5)
16	1457	1458	1492.1	1457.9	11.876	6.225	OCH3opb(81),OCH3ops(13)
17	-	1450	1483.4	1450.1	176.54	15.690	CH2SCI(94)
18	1429	1433	1477.0	1433.1	100.132	9.121	OCH3sb(70),bCCH(10)
19	1400	1401	1453.0	1401.3	520.05	16.042	CC(37),bCCH(17),CC2(15)
20	1375	-	1412.2	1378.9	118.94	84.338	bCCH(18),CC(14),bring1(10),CC(10)
21	1357	1350	1375.7	1354.1	197.649	78.072	CC (25),CO3(20),bCCH(19),OCH3sb(15)
22	1293	1292	1309.8	1283.5	474.76	65.625	CC(30),CC3(17),CC1(13),bCCH(12)
23	1271	-	1285.6	1269.3	397.87	4.000	bCCH(65),CC(8),CH2TW(6),CC(6)
24	-	1266	1272.3	1262.6	2.331	102.620	CH2TW (41),CC(24),bring1(12), bCCH (9)
25	1236	1235	1243.6	1223.6	60.907	97.010	bCCH(22),CH2ROC(13),CC(13),bring2(10)
26	1214	1216	1229.7	1218.0	182.75	86.517	CC (23),bCCH(16),CO2(13)
27	1193	-	1199.8	1196.8	7.873	98.261	CH2ROC(37),OCH3op(23),bCCH(16),CC4(6)
28	-	1183	1167.7	1179.7	11.242	4.125	OCH3ipr (22),CO2(15),CH2ROC(15),bCCH(12)
29	1143	1150	1167.1	1149.5	196.20	3.703	OCH3ipr(80),OCH3opr(14)
30	1129	1125	1158.3	1140.4	398.12	0.321	bCCH(51),CC(21),CO(9),bring1(7)
31	1057	1058	1135.9	1063.7	493.49	34.428	CC(25),CO (19),CC2(13),bring1(11)
32	1029	-	1075.2	1036.8	286.740	23.974	CO(35),CO(16),CC(12),CC(11)
33	-	1025	1045.2	1024.1	2.183	17.149	CO(23),CC(19),CC(18),CC(14)
34	990	990	999.8	982.8	144.57	17.678	CO(39),CO(20),bring2(8),CC(6)
35	960	-	963.5	961.7	51.22	0.288	gCH(89),tring2(10)
36	917	-	906.2	919.9	66.84	1.837	CC(51),gCH(12),CH2ROC(9)
37	-	868	878.4	873.1	222.55	3.641	gCH(68),gCO(9),tring1(7)
38	865	860	858.0	850.7	245.76	3.997	CO(34),tCH2(13),CC(9),gCH(6)
39	851	-	850.9	849.0	343.60	0.254	gCH(66),tring2(23),gOCO(7)
40	827	-	825.1	821.5	214.45	0.875	gCH(72),tring2(10),tring1(6)
41	800	801	805.5	800.8	112.807	17.812	bring1(36),CC2(18),bring2(14)
42	753	758	743.6	753.4	91.16	3.993	bring1(38),bring2(31),gCO(10)
43	723	725	720.5	722.5	311.01	6.690	bOC(32),tring1(7),CBr(7),gCC(7)
44	-	717	715.7	711.6	0.214	7.656	bOC(19),bring2(15),tring2(14),CC(9)
45	680	683	691.7	690.5	11.68	7.419	bring1(33),bring2(14),CC2(8)
46	667	667	668.6	667.0	21.31	8.670	CBr(17),bring2(14),bCCH(14),bCBr(10)
47	630	633	635.1	632.6	104.27	2.293	bCOC(38),tring2(34),tring1(11),gCH(6)
48	590	591	590.0	590.1	204.44	6.454	bCBr(30),bring2(19),bOC(19),CC1(8)
49	567	565	571.2	568.1	125.26	23.019	bring2(25),tring1(14),bring1(10)
50	507	508	505.8	505.1	63.68	10.598	bCC(15),tButt(14),tring1(11),bring1(10)
51	490	483	486.3	483.0	122.27	4.970	gCOC(36),bring1(21),bring2(10),bOC(8),bCO(7)
52	463	458	460.5	464.7	43.70	5.086	bring2(45),gOCO(13),tButt(10)
53	450	450	446.2	442.1	211.23	4.891	gOC(37), bOC(5)bring2(12),tring1(5),
54	-	425	424.3	422.2	2.801	21.905	bring2(27),bring1(15),CO2(11),bCO(8)
55	-	340	327.0	329.8	0.853	2.701	gCC(18),bCC(14),bring2(14),bCOC(10)

S.No.	Observed frequencies(cm^{-1})		Calculated frequencies (cm^{-1}) with B3LYP/ 6-311++G** level				PED (%) among type of internal coordinates
	Infrared	Raman	Unscaled	Scaled	IR[a] (A_i)	Raman[b] (I_i)	
56	-	305	297.2	302.5	2.414	1.234	tring1(22),tOCH3(19),tCH2(11)
57	-	283	264.8	276.6	0.076	1.359	tring1(35),tring2(30),gCH(10)
58	-	-	245.5	251.1	0.374	2.507	tring1 (23),bCC(22),tCH2(17)
59	-	216	208.4	220.5	0.530	1.048	tOCH3(42),tring1(29),tring2(10),gOCO(6)
60	-	190	195.9	196.1	2.623	2.212	tring2(24),tCBr(22),tCH2(16)
61	-	160	172.9	167.4	4.086	2.841	tring2(25),bCO(23),tCH2(15)
62	-	125	139.6	130.5	0.495	1.184	tring2(21),tCOC(19),tring1(18)
63	-	-	93.6	96.6	1.061	0.121	tButt (72),tring2(8),gCH(8)
64	-	-	87.2	76.2	2.795	1.925	tCOC(44),tOCH3(14),gCC(14)
65	-	-	59.1	49.8	2.990	2.124	tCBr(51),tCH2(42)
66	-	-	46.1	43.0	1.760	1.486	tCH2(20),tCOC(20),gCC(13)

Abbreviations used: b, bending; g, deformation; t, torsion; Butt, butterfly.
a Relative absorption intensities normalized with highest peak absorption.
b Relative Raman intensities calculated and normalized to 100.

and out-of-plane bending vibrations lies in the region 1000-400 cm^{1} (Prasad *et al.* 2013). So, the band observed at 507 cm^{1} in FT-IR and at 508 cm^{-1} in FT-Raman spectra is readily assigned for CC in-plane bending vibration. The out-of- plane vibration is allotted for the band at 340 cm^{-1} in FT-Raman spectrum.

4.5.2 C-H vibrations

The characteristic C–H stretching vibrations of heteroaromatic structure are expected to appear in 3100–3000 cm^{-1} frequency range. In infrared spectra, most of the aromatic compounds have nearly four peaks in the region 3080–3010 cm^{-1} due to ring C–H stretching bands. IR frequencies of C–H bands are a function of sp hybridization (Prabavathi *et al.* 2014). Among the four C-H stretching vibrations, three modes are identified in IR spectrum at 3010, 3030 and 3085 cm^{-1} and the fourth in Raman at 3075 cm^{-1}. These vibrations are in good agreement with the calculated values, with an average of 98% PED contribution.

The C–H in-plane-bending vibrations are usually expected to occur in the region 1300–1000 cm^{-1} and these vibrations are very useful for characterization purposes (Pavia *et al.* 2001). The calculated values 1140, 1263, 1271 and 1375 cm^{-1} are assigned to four C–H in-plane-bending vibrations. All the four peaks are present in FTIR spectrum at 1129, 1236, 1271 and 1375 cm^{-1}. The C–H out-of-plane bending vibrations are strongly coupled and occur in the region

Table 6. Experimental and Theoretical isotropic chemical shifts (with respect to TMS, all values in ppm) for 7-methoxy-4-bromomethylcoumarin

Atom	Chemical Shift (ppm)	
	Calculated	Experimental
C 7	170	163
C 9	164	161
C 2	164	156
C 4	160	150
C 5	132	126
C 6	118	114
C 3	116	113
C 10	115	111
C 8	102	101
C 20	56	56
C 13	46	27
H 17	8.1	7.6
H 18	7.1	7.3
H 24	6.8	6.8
H 12	6.1	6.4
H 15	4.7	4.4
H 21	4.2	3.8
H 14	4.1	4.4
H 22	3.8	3.8
H 23	3.8	3.8

Table 7. The Second-order perturbation energies $E^{(2)}$ (Kcal/mol) corresponding to the most important charge transfer interactions (donor-acceptor) in 7-methoxy-4-bromomethylcoumarin by B3LYP/6-311++G method**

Excited state	Wavelength λ (nm)	Excitation energies (eV)	Oscillator strengths (f)
S1	338.6	3.66	0.29
S2	214.3	5.78	0.13
S3	201.4	6.15	0.42
S4	200.7	6.17	0.22

Table 8. The Second-order perturbation energies E(2) (Kcal/mol) corresponding to the most important charge transfer interactions (donor-acceptor) in 7-methoxy-4-bromomethylcoumarin by B3LYP/6-311++G method.**

NBO(i)	ED/e	NBO(j)	Type	ED/e	E(2)[a] (kJmol)	E(j)–E(i)[b] (a.u.)	F(i, j)[c] (a.u.)	ED_A(%) (a.u) of j	ED_B(%) (a.u) of j
(σ) O1-C2	1.99011	C10-C5	σ*	0.02303	18.32	1.09	0.127	48.26	51.74
		C10-C9	σ*	0.03493	38.56	0.85	0.162	49.15	50.85
		C6-H18	σ*	0.01250	10.86	1.18	0.101	38.80	61.20
		C7-C8	σ*	0.02723	18.51	1.19	0.133	50.06	49.94
(σ) O1-C9	1.98957	C2-O11	σ*	0.01228	40.98	0.68	0.161	64.43	35.57
		C3-C4	σ*	0.01943	51.22	1.05	0.208	50.96	49.04
		C10-C5	σ*	0.02303	66.84	1.17	0.250	48.26	51.74
		C10-C9	σ*	0.03493	126.84	0.92	0.307	49.15	50.85
		C6-H18	σ*	0.01250	23.02	1.26	0.152	38.80	61.20
		C7-C8	σ*	0.02723	23.17	1.26	0.153	50.06	49.94
(σ) C2-C3	1.98139	C3-C4	σ*	0.01943	43.70	0.81	0.168	50.96	49.04
		C10-C5	σ*	0.02303	16.73	0.93	0.110	48.26	51.74
		C10-C9	σ*	0.03493	37.73	0.68	0.144	49.15	50.85
(σ) C2-O11	1.99444	C7-C8	π*	0.37600	740.72	0.03	0.149	56.11	43.89
(σ) C3-C4	1.97452	C2-O11	σ*	0.01228	12.49	1.23	0.111	64.43	35.57
		C2-O11	π*	0.28458	12.88	0.52	0.076	68.90	31.10
		C3-C4	σ*	0.01943	16.39	0.90	0.108	50.96	49.04
		C20-H21	σ*	0.00847	13.71	4.09	0.212	40.08	59.92
		C20-H22	σ*	0.01736	10.70	3.74	0.179	40.81	59.19
(π) C3-C4	1.80408	C3-C4	σ*	0.01943	22.89	0.41	0.091	50.96	49.04
		C10-C9	σ*	0.03493	20.01	0.28	0.069	49.15	50.85
(σ) C3-H12	1.97516	C2-O11	π*	0.28458	14.90	0.28	0.062	68.90	31.10
(σ) C4-C10	1.96776	C10-C5	σ*	0.02303	27.54	0.91	0.141	48.26	51.74
(σ) C10-C5	1.96829	C10-C5	σ*	0.02303	14.89	0.91	0.104	48.26	51.74
		C10-C5	σ*	0.02303	32.03	0.93	0.155	48.26	51.74
(σ) C10-C9	1.96990	C10-C9	σ*	0.03493	24.94	0.69	0.117	49.15	50.85
		C7-C8	σ*	0.02723	17.73	1.03	0.121	50.06	49.94
(σ) C5-C6	1.97616	C10-C9	σ*	0.03493	38.32	0.69	0.145	49.15	50.85
		C7-C8	σ*	0.02723	17.55	1.03	0.120	50.06	49.94
LP(1) O19	1.96288	C7-C8	σ*	0.02723	41.15	0.87	0.169	50.06	49.94

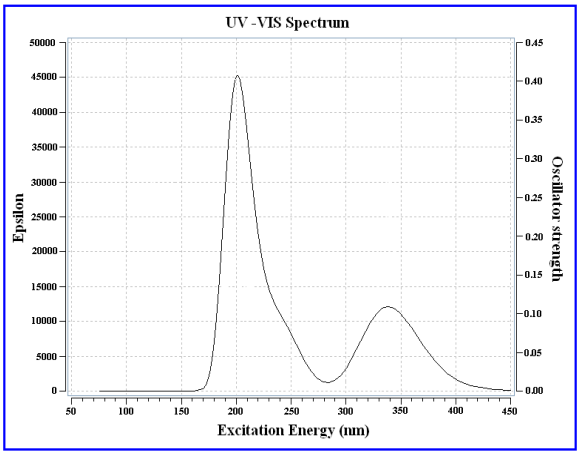

Fig. 11. Theoretically calculated UV-Vis spectrum of 7-methoxy-4-bromomethylcoumarin

1000 to 700 cm^{-1} (Prabavathi *et al.* 2014). Accordingly, the calculated values are assigned as shown in Table 5..

4.5.3 Bromomethyl vibrations

The C-Br stretching vibration computed at 667 cm^{-1} exactly coincide the experimental value, in both IR and Raman spectrum. The vibrational frequencies and IR intensities of CH_2-Br group are sensitive to conformational changes and nature of substituent (El-Nahass *et al.* 2011). The CH_2-Br asymmetric stretching vibration is identified at 2975 cm^{-1} in Raman and the findings given in the literature (Prabhavathi *et al.* 2014) supports this assignment. The CH_2-Br symmetric stretching vibration appears in FT-IR and FT-Raman spectra at 2950 and 2942 cm^{-1}, respectively. The fundamental CH_2-Br vibrations due to scissoring, wagging, twisting and rocking appear in the

frequency region 1500– 800 cm^{-1} (Silverstein *et al.* 1981). In light of the above statement the computed values at 1197, 1269 and 1450 cm^{-1} were assigned for CH_2-Br rocking, twisting and scissoring vibrations, respectively. Among the vibrations mentioned above, the rocking mode vibration is present in IR spectrum at 1193 cm^{-1} and the other two vibrations were found in Raman at 1266 and 1450 cm^{-1} respectively.

4.5.4 C-O Vibrations

The C=O group vibrations are likely to be the most sensitive to the environment. Hence, they show pronounced shifts in the spectra of the aromatic compounds. The C=O stretching band is characterized by a very strong and sharp band appearing approximately at 1700 cm^{-1}(Balachandran and Karunakaran, 2013). So, for 7BMC the C2=O11 stretching vibration is allotted for the simulated value 1720 cm^{-1} and its experimental counterpart in IR spectrum exactly coincide with this value.The two ring CO stretching vibrations (C9-O1 and C2-O1) are predicted at 851 and 983 cm^{-1}. Both of these vibrations are found in IR at 865 and 990 cm^{-1}, respectively. The methoxy group C-O stretching vibrations are calculated at 1024 and 1037 cm-1. Out of these twobands, one is found in IR spectrum alone at 1029 cm^{-1} and the other is present in Raman spectrum only at 1025 cm^{-1}.

4.5.5 Methoxy group vibrations

The compound selected for the present study has one methoxy group substituted in the 7th position of the titled molecule. For the assignments of CH_3 group frequencies, one can expect that nine fundamentals can be associated to CH_3 group namely CH_3ss, symmetric stretch; CH_3ips, in-plane stretch (i.e. in-plane hydrogen stretching mode); CH_3 ipb, in-plane bending, (i.e. hydrogen deformation mode); CH_3sb, symmetric bending; CH_3 ipr, in-plane rocking; CH_3opr, out-of plane rocking; CH_3 ops, out-of-plane stretch; CH_3 opb, out-of plane bending modes and tCH_3 twisting modes. Among which the CH_3ops, out-of-plane stretch and CH_3opb, out-of plane bending modes of CH_3 group would be expected to be depolarized for A" symmetry species. In addition to this OC wagging and C–O–C in-plane bending also exist. The CH_3 symmetric and asymmetric stretching vibrations generally occur at lower frequency region 2850–3000 cm^{-1}. The out-of-plane stretching mode of CH3 group is expected around 2980 cm^{-1} and symmetric one is expected around 2870 cm^{-1}(Krishnakumar and Prabhavathi, 2010). For the title compound the peaks identified in IR at 2920 and 2860 cm^{-1} and in FT-Raman at 2850 cm^{-1} are attributed to CH_3ops, CH_3 ips, and CH_3ss vibrations respectively.

For methyl substituted benzene derivatives the antisymmetric and symmetric deformation vibrations of methyl group normally appear in the region 1465–1440 cm^{-1} and 1390–1370 cm^{-1} respectively and the rocking vibrations of CH3 modes usually appear in the region 1070–1010cm^{-1} (Krishnakumar and Prabhavathi, 2010). Based on the above data the bands found in FT-Raman at 1150,1183,1433, 1458 and 1517 cm^{-1} are assigned for the vibrations OCH_3opr, OCH_3ipr, OCH_3sb, OCH_3opb and OCH_3ipb, respectively. The torsional vibration (tOCH3) evaluated at 221 cm^{-1} was found in Raman spectrum at 216 cm^{-1}. The experimental values agree well the simulated values.

4.6 NMR Analysis

The experimental values for ^{1}H and ^{13}C NMR of 7BMC were measured in $CDCl_3$solution. The ^{1}H and ^{13}C theoretical and experimental chemical shifts are tabulated in Table 6. The correlation coefficient for proton (0.991) and carbon (0.993) chemical shift is calculated from linear regression curves. These values confirm the good agreement between experimental and calculated chemical shift values. The theoretical ^{13}C and ^{1}H NMR spectra of 7BMC and their respective linear regression curves were depicted in Fig. 6 and Fig. 7, respectively. Hydrogen attached to near by electron withdrawing atom or group can decrease the shielding and move the resonance of attached proton towards a higher frequency. By contrast electron donating atom or group increases the shielding and moves the resonance towards to a lower frequency (Sebastin *et al.* 2011). Accordingly for 7BMC the chemical shift value of $-CH_2Br$ and $-OCH_3$ attached H atom experiences a lesser value of about 3.8 to 4.4 ppm and fairly agrees with the calculated value. The other four hydrogen atoms attached to ring carbons have a greater value.

Aromatic carbon gives signals with chemical shift values from 100 to 200 ppm (Prabhavathi and Senthil Nayaki, 2014). Except C13 and C20 atoms, the chemical shift values of all the carbons of 7BMC are in accordance with the above statement. The shielding around C13 atom in bromomethyl group and C20 atom in methoxy group of 7BMC is somewhat high enough compared to other carbon atoms due to the presence of nearby electronegative atoms. So the chemical shifts of those carbons are set upfield with a low ppm value of about 27 and 56 ppm respectively.

4.7 UV-Vis Spectral Analysis

The time-dependent density functional theory (TD-DFT) calculation has been performed to investigate the electronic absorption properties of 7BMC. The calculated visible absorption maxima (λ_{max}) which are the functions of electron availability, theoretical electronic excitation energies and oscilla-tor strength are all tabulated in Table 7. The theoretically calculated UV-VIS spectrum is depicted in Fig. 11. The calculated λ_{max} values for 7BMC are 338.6, 214.3, 201.4 and 200.7nm, among which very strong light absorptions at 214.3, 201.4 and 200.7 nm are due to $\pi \rightarrow \pi^*$ transitions. The absorption band of 7BMC at the longer wave length region 338.6 nm is caused by the $n–\pi^*$ transition. This type of transition is the characteristic nature of compounds containing double bonds involving hetero atoms (e.g., C=O).

4.8 Natural Atomic Charges

The calculation of effective atomic charges plays an important role in the application of quantum mechanical calculation to molecular systems. The calculated natural atomic charge values from the natural population analysis (NPA) are portrayed in the Fig. 8. Natural atomic charges analysis chart is shown in Fig. 9. From the figures, it is evident that there is no difference in charge distribution observed on all the hydrogen atoms. The methoxy group hydrogen atoms show a slightly less value which is not appreciable. The carbon atoms C2, C7 and C9 exhibit positive charges due to the presence of electronegative oxygen atoms in their neighbourhood. The neutral charge on C4 and Br16 atom shows the pinnacle delocalization of their charges towards C14 atom. So, C14 is more negative than the other carbon atoms of 7BMC. The charge on the oxygen atoms of 7BMC averages to -0.5.

4.9 Frontier Molecular Orbitals

Frontier molecular orbitals (FMOs) play an important role in the optical and electronic properties, as well as in quantum chemistry and UV–Vis spectra. The HOMO represents the ability to donate an electron where LUMO, as electron acceptor, represents the ability to obtain electron and the energy gap between HOMO and LUMO characterizes the molecular chemical stability, chemical reactivity, hardness and softness of the molecule (Sylystree *et al*. 2012). The three dimensional plots of the FMOs are shown in Fig. 10.

The highest occupied molecular orbitals are localized mainly on the parent ring and the methoxy group. The LUMO plot is almost uniformly distributed except the methoxy group. The HOMO and LUMO transition implies an electron density transfer from the coumarin ring to the bromomethyl group. The transition from HOMO to LUMO of the molecule results in the energy gap (ΔE) of about 2.945 eV. From the energy gap value it can be shown that the titled compound has low band gap energy. Thus the molecule 7BMC implies high chemical reactivity, because it is energetically favorable to add electron to a high-lying LUMO by extracting electrons from low-lying HOMO (Aihara, 1999).

4.10 NBO Analysis

Table 8 depicts the bonding concepts such as type of bond orbital their occupancies, the natural atomic hybrids and the percentage of the NBO on each hybrid of 7BMC molecule determined by B3LYP/6-311++G** method. The occupancies of NBO's in 7BMC reflect their exquisite dependence on the chemical environment. The NBO energy values show the corresponding spatial symmetry breaking in the direction of unpaired spin. The most important bond–antibonds and lone-pair–antibonds interaction energies of 7BMC are given in Table 8. The intra-molecular interaction is formed by the orbital overlap between σ (C–C) and σ^* (C–C) bond orbital which results intra-molecular charge transfer (ICT) causing stabilization of the system. These interactions

are observed as increase in electron density (ED) in C–C antibonding orbital that weakens the respective bonds.The strongest delocalization in 7BMC is between σ (C2-O11)→ (C7-C8) and σ (O1-C9) →σ*(C10-C9). These interactions stabilize the titled molecule by 740.7 kJ/mol and 126.8 kJ/mol, respectively. The other interactions producing a large stabilizing energies are σ (O1-C9) →σ* (C10-C5), σ (O1-C9)→ σ* (C3-C4) and σ (C2-C3) →σ* (C3-C4), with energies of about 66.84, 51.22& 43.7 kJ/mol respectively.

5. CONCLUSION

In this study, the optimized molecular structure, PED, thermodynamicand electronic properties of the title compound are calculatedby DFT method using B3LYP/6-311G(d,p) basis set. Thecomplete molecular structural parameters and thermodynamicproperties of the compound have been calculated. The correlations between the statistical thermodynamics and temperature are also obtained. It was seen that the entropies and enthalpies increase with the increase in temperature as the intensities are enhanced by the higher temperature values. The fundamental vibrationalmodes of the title compound have been precisely assigned, analyzed and the experimental results were compared withthe theoretical values. As the β_{tot} value of the compound is high, 7BMC can be used as a good NLO material. The molecule 7BMC shows high chemical reactivity which is evident from the low band gap energy. The influences of electronegative atoms on the atomic charges werestudied in detail. The prediction of reactive behaviorof 7BMC in both electrophilic and nucleophilic reactions has been done with the help of MESP visualization. The chemical shift shielding tensors were predicted by the computational NMR method. Thus the complete vibrational assignments, structural information and electronic properties of the titled compound were provided in the present investigation.

ACKNOWLEDGEMENT

We are thankful to Sophisticated Analytical Instrumentation Facility (SAIF), IIT Madras, Chennai, and St. Joseph's college, Thiruchirappalli, India for providing generous support in taking spectral measurements.

REFERENCES

Aihara, J., Reduced HOMO LUMO gap as an index of kinetic stability for polycyclic aromatic hydrocarbons, *J. Phys. Chem.A.*, 103, 7487–7495(1999). doi:10.1021/jp990092i

Alekseev, S. M., Pomoinitskii, V. D., Sarycheva, I. K., Evstigneeva, R. P., Use of 4-bromomethyl-7-methoxycoumarin for the quantitative fluorometric analysis of prostaglandins, *Pharm. Chem. J.*, 15(11), 825-827(1981). doi:10.1007/BF00760468

Arjunan, V., Arushma Raj, Ravindran, P., Mohan, S., Structure–activity relations of 2- (methylthio) benzimidazole by FTIR, FT-Raman, NMR, DFT and conceptual DFT methods, *Spectrochim. Acta.*, 118, 951–965(2014). doi:10.1016/j.saa.2013.09.100

Arjunan, V., Sakiladevi, S., Marchewka, M. K., Mohan, S., FTIR, FT-Raman, FT-NMR and quantum chemical investigations of 3-acetylcoumarin, *Spectrochim. Acta*, 109, 79-89(2013). doi:10.1016/j.saa.2013.01.100

Balachandran, V., Karunakaran, V., Quantum mechanical study of the structure and vibrational spectroscopic (FT-IR and FT-Raman), first-order hyperpolarizability, NBO and HOMO LUMO studies of 4-bromo-3-nitroanisole, *Spectrochim. Acta.*, 106, 284-298(2013). doi:10.1016/j.saa.2012.12.070

Benito Reyes-Trejo, Diana Guerra-Ramirez, Holber Zuleta-Prada, Rosa Santillan, Maria Elena Sanchez-Mendoza, Jesus Arrieta and Lino Reyes, Molecular Disorder in (-)-Encecanescin, *Molecules*, 19, 4695-4707(2014). doi:10.3390/molecules19044695

Borges, F., Roleira, F., Milhazes, N., Santana, L., Uriarte, E., Simple coumarins and analogues in medicinal chemistry: Occurrence, synthesis and biological activity, *Curr. Med. Che.*, 12, 887-916(2005). doi:10.2174/0929867053507315

Elbert, W., Breitenbach, S., Neftel, A., Hahn, J., 4-methyl-7-methoxycoumarin as a fluorescent label for high-performance liquid chromatographic analysis of dicarboxylic acids, *J. Chromatogr.* A, 328, 111-120(1985). doi:10.1016/S))21-9673(01)87382-9

El-Nahass, M. M., Kamel, M. A., El-Deeb, A. F., Atta, A. A. and Huthaily, S. Y., Density functional theory (DFT) investigation of molecular structure and frontier molecular orbitals (FMOs) of P-N,N-dimethylaminobenzylidenemalononitrile (DBM), *Spectrochim. Acta*, 79, 1499–1504(2011). doi:10.1016/j.saa.2011.05.006

Krishnakumar, V. and Prabavathi, N., Structure and vibrational frequencies of 6,7-dimethoxy-1,4-dihydro-1,3-quinoxalinedione based on density functional theory calculations: The role of ð-electron conjugation and back-donation, *Spectrochim. Acta*, 77, 238-247(2010). doi:10.1016/j.saa.2010.05.015

Pavia, D. I., Lampman, G. M. and Kriz, G. S., Introduction to spectroscopy: A guide for student of organic chemistry, *Physics, in: J. Vondeling (Ed.)*, third ed., Thomson, Learning(2001).

Prabavathi, N., Nilufer, A. and Krishnakumar, V., FT-IR, FT-Raman and DFT quantum chemical study on the molecular conformation, vibrational and electronic transitions of 1-(m-(trifluoromethyl) phenyl) piperazine, *Spectrochim. Acta.*, 121, 483-493(2014). doi:10.1016/j.saa.2013.10.102

Prabavathi, N., Nilufer, A. and Krishnakumar, V., Vibrational spectroscopic (FT-IR and FT-Raman) studies, natural bond orbital analysis and molecular electrostatic potential surface of Isoxanthopterin, *Spectrochim. Acta.*, 114,101-113(2013). doi:10.1016/j.saa.2013.05.013

Prabavathi, N. and Senthil Nayaki, N., Molecular structure, FT-IR, FT-Raman, NMR studies and first order molecular hyperpolarizabilities of 7-methoxy-4-methylcoumarin by DFT Method, *Phys. Express.*, 4(12), 1-15 (2014).

Prasad, M. V. S., Kadali Chaitanya, Udaya Sri, N. and Veeraiah, V., Experimental and theoretical (HOMO, LUMO, NBO analysis and NLO properties) study of 7-hydroxy-4-phenylcoumarin and 5,7-dihydroxy-4-phenylcoumarin, *J. Mol. Struct.*, 1047, 216–228(2013). doi:10.1016/j.molstruc.2013.04.066

Sebastian, S., Sundaraganesan, N., Karthikeiyan, B. and Srinivasan, V., Quantum mechanical study of the structure and spectroscopic (FT-IR, FT-Raman, ^{13}C, ^{1}H and UV), first order hyperpolarizabilities, NBO and TD-DFT analysis of the 4-methyl-2-cyanobiphenyl, *Spectrochim. Acta.*, 8, 590–600(2011). doi: 10.1016/j.saa.2010.11.028

Sebastian, S., Sylvestre, S., Sundaraganesan, N., Amalanathan, M., Ayyapan, S., Oudayakumar, K. and Karthikeyan, B., Vibrational spectra, molecular structure, natural bond orbital, first order hyperpolarizability, TD-DFT and thermodynamic analysis of 4-amino-3- hydroxy-1-naphthalene sulfonic acid by DFT approach, *Spectrochim. Acta.*, 107, 167-178(2013). doi:10.1016/j.saa.2013.01.041

Sheela, N.R., Muthu, S. and Sampathkrishnan, S., Molecular orbital studies (hardness, chemical potential and electrophilicity), vibrational investigation and theoretical NBO analysis of 4-4ˈ-(1H-1,2,4-triazol-1-yl methylene) dibenzonitrile based on abinitio and DFT methods, *Spectrochim. Acta.*, 120, 237–251(2014). doi:10.1016/j.saa.2013.10.007

Silverstein, M., Clayton Basseler, G. and Morill, C., Spectrometric Identification of Organic Compound, Wiley, New York, 1981.

Sylvestre, S., Sebastian, S., Oudayakumar, K., Jayavarthanan, T. and Sundaraganesan, N., Experimental (FT-IR, FT-Raman and UV–Vis) spectra and theoretical DFT investigations of 2,3-diaminophenazine, *Spectrochim. Acta.*, 96, 401–412(2012). doi:10.1016/j.saa.2012.05.047